



Synergistic promotion on photoactivity and stability of $W_{18}O_{49}/TiO_2$ hybrid

Zhen-Feng Huang, Ji-Jun Zou*, Lun Pan, Songbo Wang, Xiangwen Zhang, Li Wang

Key Laboratory for Green Chemical Technology of the Ministry of Education, School of Chemical Engineering and Technology, Tianjin University, Tianjin 300072, China

ARTICLE INFO

Article history:

Received 23 May 2013

Received in revised form 22 August 2013

Accepted 25 August 2013

Available online 31 August 2013

Keywords:

$W_{18}O_{49}$

TiO_2

Photocatalysis

Hybrid photocatalyst

Hetero-junctions

ABSTRACT

Hybrid photocatalysts were constructed by mixing $W_{18}O_{49}$ with commercial TiO_2 (P-25) and tested for photodegradation of pollutants (methyl orange and phenol). $W_{18}O_{49}$ synthesized by alcoothermal method possesses urchin-like structure, high surface area of $178\text{ m}^2\text{ g}^{-1}$ and wide light absorption in 200–800 nm. Although $W_{18}O_{49}$ alone shows low photoactivity, the hybrid shows significant synergistic promotion. The activity of $W_{18}O_{49}(10\text{ wt\%})/TiO_2$ under UV-vis light and $W_{18}O_{49}(90\text{ wt\%})/TiO_2$ under visible light is 2.43 (2.64) and 1.31 (1.52) times of calculated value without considering the synergy for the degradation of MO (phenol), respectively. Controlled experiments indicate $\cdot O_2^-$ from reduction of O_2 by photo-induced electrons is the key active species in the photodegradation. The synergy was attributed to the well-matched band structure of two semiconductors that enhances charge separation, with electrons moving to $W_{18}O_{49}$ and holes to TiO_2 , as confirmed by photo-deposition of Au and PbO_2 . Furthermore, $W_{18}O_{49}/TiO_2$ is much more active than WO_3/TiO_2 attributed to the good reductive capability and wide light absorption of oxygen vacancies in $W_{18}O_{49}$. Moreover, the unstable $W_{18}O_{49}$ shows excellent stability in the hybrid.

© 2013 Elsevier B.V. All rights reserved.

1. Introduction

Recent years, solar-light-induced photocatalysis based on semiconductor has seen a renewed interest in the fields of degradation of pollutants, water splitting, CO_2 reduction, solar cells and so on [1,2]. Specifically, TiO_2 is the most widely studied photocatalyst due to its low cost, chemical stability, and nontoxicity [3–5]. However, it suffers from some drawbacks such as wide band gap utilizing only UV light and fast charge recombination suppressing the quantum efficiency. Many strategies have been developed to modify TiO_2 and overcome these problems, such as metal and nonmetal doping [6,7], surface sensitization [8–10], and composite/hybrid with hetero-junctions [11–13]. Importantly, composite or hybrid semiconductor, via coupling TiO_2 with other semiconductors possessing suitable band structures (i.e., CdS and Fe_2O_3), can enhance the separation of photo-induced charge by forming well-matched band structures or p–n junctions [14–18].

Narrow-bandgap semiconductors can absorb visible light that accounts for 40% of solar energy. Recently, metallic oxides with oxygen vacancies have attracted great interest due to their distinctive defect structures [1,13,19]. Among them, $W_{18}O_{49}$ shows a wide absorption tail in near infrared region, thus very promising

as visible photocatalyst [19,20]. For instance, $W_{18}O_{49}$ nanowires show remarkable activity in CO_2 reduction under visible light [19]. Unfortunately, the efficiency of narrow-bandgap photocatalysts is relatively low due to the inherent fast charge recombination. Moreover, their photo-stabilities are susceptible because the oxidation and/or reduction potentials often lie within the band levels that induces photo-oxidation and/or reduction. Still for $W_{18}O_{49}$, in the photocatalytic CO_2 reduction, it is prone to deactivation owing to the formation of WO_3 arising from photo-oxidation by holes accumulated in the valence band [19]. Therefore, breaking the trade-off between light harvesting and charge separation, along with the stability, is vital for the application of narrow-bandgap photocatalysts. Recent efforts have been directed toward surface decoration of $W_{18}O_{49}$ with $Ag/AgCl$ and carbon, which significantly promote the photoactivity [21–23].

Actually, TiO_2 is a promising photo-oxidation photocatalyst because of the strong oxidizing ability of valence holes, and in most cases it shows higher photoactivity than other semiconductors under UV irradiation. In contrast, narrow-bandgap photocatalysts are capable of harvesting visible light, although the activity needs promotion. Therefore, coupling TiO_2 with narrow-bandgap photocatalysts may cover both UV and visible light more efficiently. Moreover, when their band structures are properly matched, the photo-induced charge separation can be enhanced and the charge recombination and photo-corrosion can be inhibited. With this consideration, in this work, we construct $W_{18}O_{49}/TiO_2$ hybrid by

* Corresponding author. Tel.: +86 22 27892340; fax: +86 22 27892340.

E-mail address: jj.zou@tju.edu.cn (J.-J. Zou).



mixing the two semiconductors together, investigate the synergistic promotion on the photoactivity and stability, and explain the synergy by determining the active species and charge separation pathway. This work may be helpful for understanding the synergistic effect of composite/hybrid and designing highly active materials with desirable hetero-junctions for environmental remediations.

2. Experimental

2.1. Materials

Tungsten(VI) hexachloride, nitroblue tetrazolium (NBT), phenol and benzoquinone (BQ) were obtained from J&K Chemical. Methyl orange (MO), C_2H_5OH , $HAuCl_4 \cdot 4H_2O$, tert-butyl alcohol (TBA), ammonium oxalate (AO) and $Pb(NO_3)_2$ were purchased from Tianjin Guangfu Fine Chemical Research Institute. Commercial TiO_2 (P-25) was from Degussa: Hulls Corporation. All the reagents were reagent grade and used as received.

2.2. Photocatalyst preparation

$W_{18}O_{49}$ was prepared by alcoholysis of WCl_6 according to the literature [20]. Typically, 1.6 g of WCl_6 was dissolved in 80 mL of absolute ethanol. The transparent solution was transferred to a 100 mL Teflon-lined stainless steel autoclave and heated at 160 °C for 24 h. The resultant products were collected, followed by washing with deionized water and ethanol for 3 times, and finally dried at 40 °C overnight. WO_3 was prepared by calcining the as-prepared powders at 420 °C for 30 min with a heating rate of 1 °C/min. $W_{18}O_{49}/TiO_2$ and WO_3/TiO_2 hybrids were obtained by simply mixing the related semiconductors.

2.3. Characterizations

The crystal structures were recorded using a Rigaku D/max-2500 X-ray diffractometer (XRD) equipped with a Cu K α irradiation source. The BET surface area was determined using N_2 adsorption/desorption isotherm measurements at -196 °C on a Micrometrics TriStar 3000 equipment. The morphology and microstructure were examined on a Tecnai G² F20 transmission electron microscopy (TEM) operated at 200 kV and a Nanosem 430 field emission scanning electron microscopy (SEM). UV-vis diffuse reflectance spectra (UV-vis DRS) were recorded with a Hitachi U-3010 spectrometer equipped with a 60 mm diameter integrating sphere using $BaSO_4$ as the reference.

2.4. Photoactivity measurements

The photodegradation of MO and phenol were conducted in aqueous solution vertically irradiated by a 300 W high-pressure xenon lamp (PLS-SXE-300UV, Beijing Trusttech. Co. Ltd.). The UV-vis (200–800 nm) and visible light (420–800 nm) were separated by vis-ref and UV-cut optical filters, respectively. The intensity is 37.0 mW cm⁻² at 365 nm for UV-vis light, and 43.0 mW cm⁻² at 420 nm for visible light. The irradiation area of the light source was ca. 20 cm². The reactor was open to air in order to reach the air-equilibrated condition. Typically, 20 mg of photocatalyst were dispersed in 100 mL MO (0.12 mM) or phenol (0.2 mM) solution with magnetic stirring. Prior to the irradiation, the suspension was stirred for 20 min in the dark to ensure the adsorption equilibrium. The reaction temperature was controlled at 25 °C with no acid or alkaline reagents added. During the reaction, samples were withdrawn at intervals, centrifuged, and analyzed. The concentration of residual was determined using a Hitachi U-3010 UV-vis spectrometer by monitoring the characteristic absorption

wavelength of 463 nm for MO or 270 nm for phenol, and the data were fitted using a pseudo-first-order kinetic equation to obtain the reaction rate constant (k). In addition, the total organic carbon (TOC) of some samples was measured by a Shimadzu TOC-V_{CPH} analyzer.

To evaluate the role of different active species in the photocatalytic reaction, controlled experiments using different radical scavengers (AO as scavenger for photo-induced holes (h^+), TBA for hydroxyl radicals ($\cdot OH$) and BQ for superoxide radicals ($\cdot O_2^-$), respectively) were performed under UV-vis light [24]. The reaction conditions were similar to the photodegradation except that additional radical scavengers (0.1 mM) were added into the reaction mixture.

The $\cdot O_2^-$ generated in the photocatalytic reaction was measured using NBT as probe molecule [25]. The reaction conditions were similar to the photodegradation except replacing MO using NBT (5×10^{-5} M).

2.5. Photo-deposition of Au and PbO_2

Photo-deposition of Au and PbO_2 were conducted using photo-reduction and photo-oxidation methods, respectively [26–29]. Typically, 50 mg of catalyst was dispersed in 30 mL aqueous solution containing 0.78 mg L⁻¹ $HAuCl_4$ or 2 mg L⁻¹ $Pb(NO_3)_2$ with magnetic stirring. After irradiation under UV-vis light for 30 min, the powders were separated, washed and dried at room temperature.

3. Results and discussion

3.1. Structure of $W_{18}O_{49}$ and WO_3

XRD patterns in Fig. 1a reveal that the samples obtained by alcoholysis of WCl_6 are monoclinic phase $W_{18}O_{49}$ (JCPDS No. 36-101). Only two obvious diffraction peaks corresponding to the (0 1 0) and (0 2 0) plane appear at 23.4° and 47.5°, respectively. After thermal calcination, $W_{18}O_{49}$ is converted to monoclinic phase WO_3 (JCPDS No. 43-1035). To confirm the XRD results, the Raman spectra were recorded to distinguish the different phases of tungsten oxides (Fig. 1b). Generally, $W_{18}O_{49}$ contains a wide range of W–O–W bond lengths, so the Raman spectra should show very broad and featureless bands [30,31]. Indeed, $W_{18}O_{49}$ in the present work shows only two broad peaks located at 100–400 and 600–900 cm⁻¹, in agreement with the general characteristics of $W_{18}O_{49}$ [15,26]. Meanwhile, WO_3 shows four characteristic peaks centered at 805, 715, 324, and 270 cm⁻¹, which also agrees with the literatures [19,30,32].

SEM and TEM images (Fig. 2a and b) show the as-synthesized $W_{18}O_{49}$ has urchin-like structure assembled between many nanowires with diameter less than 20 nm and length in the range of 500–600 nm. HRTEM image (Fig. 2c) confirms that the $W_{18}O_{49}$ nanowires are single crystalline. The ordered crystal fringes are indexed to the (0 1 0) planes of monoclinic $W_{18}O_{49}$ according to the spacing of 0.37 nm [19,20]. This indicates that the growth direction of nanowire is along the [0 1 0] axis. In addition, the urchin-like $W_{18}O_{49}$ possesses a high BET surface area of 178 m² g⁻¹ determined by N_2 adsorption and desorption isotherms. Likewise, WO_3 also shows the urchin-like morphology (Fig. 2d) and has a high BET surface area of 169 m² g⁻¹. This indicates the thermal calcination does not influence the textural structure of prepared materials.

From the UV-vis diffuse reflectance spectrum (Fig. 3), $W_{18}O_{49}$ exhibits a very wide absorption range from UV to visible light, which is attributed to the presence of oxygen vacancies [20,33]. In contrast, the absorption edges of WO_3 and TiO_2 are at 460 and 387 nm, respectively.

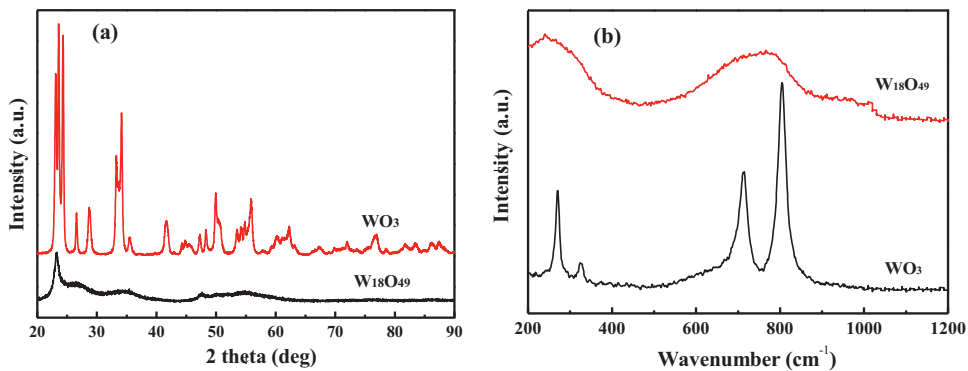


Fig. 1. (a) XRD patterns and (b) Raman spectra of W₁₈O₄₉ and WO₃.

3.2. Photoactivity under UV-vis light

The photoactivity of the samples was evaluated by the degradation of dyes (MO) and organics (phenol) under UV-vis light, respectively. The effects of absorption of reactant by photocatalyst and photolysis of reactant were excluded by blank experiments (see Fig. 4a and c). In addition, the concentration of MO (phenol) remained in the irradiated samples determined by both UV-vis spectrometer and TOC measurement change in the same tendency with the increase of irradiation time, which confirms that the pollutants are mineralized to CO₂ by photocatalysis.

As shown in Fig. 4b and d, the photoactivity of individual semiconductor (W₁₈O₄₉, WO₃ or TiO₂) is relatively low, due to the fast charge combination. Specifically, pure W₁₈O₄₉ shows very low activity when compared with TiO₂, indicating the charge combination is a big problem for narrow-bandgap semiconductors.

Fortunately, W₁₈O₄₉/TiO₂ hybrid formed by physically mixing shows obviously enhanced activity. We calculated the expected activity (K_c) as follows: (Eq. (1))

$$K_c = (K_W \times W_W) + (K_T \times W_T) \quad (1)$$

where K_W and K_T are respectively assigned to the reaction rates of pure W₁₈O₄₉ and TiO₂, and W_W and W_T are assigned to the corresponding weight ratio. This is a benchmark to show the expected activity when there is no any interaction between the two semiconductors. It is observed that the hybrids with different composition are always more active than the benchmark, indicating that a synergy between W₁₈O₄₉ and TiO₂ exists. On one hand, the addition of small amount of W₁₈O₄₉ (W_W from 0 to 10 wt%) can significantly improve the activity of TiO₂. Specifically, adding 10% of W₁₈O₄₉ gives the highest activity, which is 2.25 (2.4) times of pure TiO₂ and 2.43 (2.64) times of the benchmark for the degradation of MO

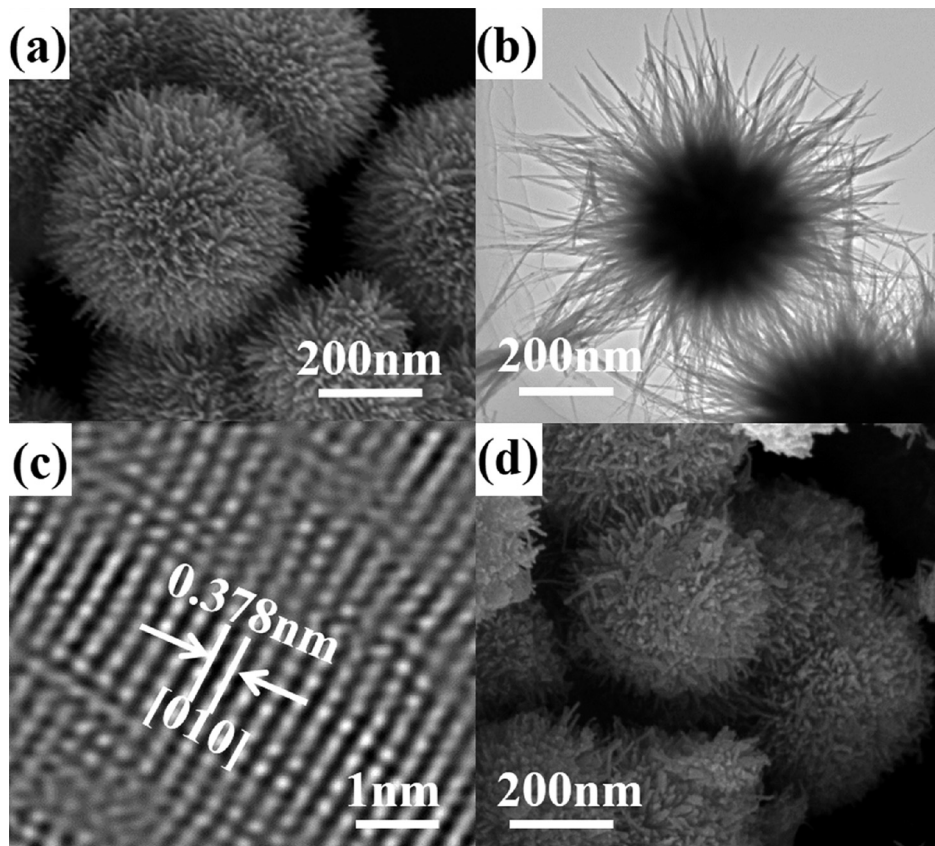


Fig. 2. (a) SEM and (b, c) TEM images of W₁₈O₄₉, and (d) SEM image of WO₃.

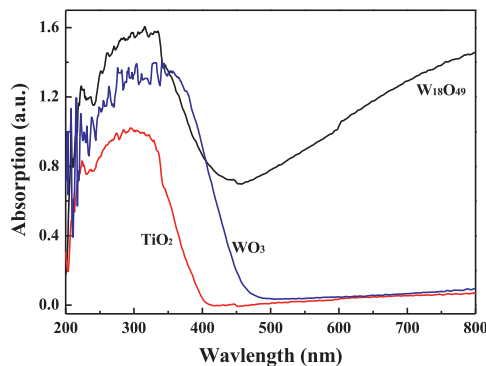


Fig. 3. UV-vis diffuse reflectance spectrum of $\text{W}_{18}\text{O}_{49}$, WO_3 and TiO_2 .

(phenol). On the other hand, with the addition of small amount of TiO_2 (W_W from 100 to 90 wt%), the activity of $\text{W}_{18}\text{O}_{49}$ is also increased. This synergy is very likely owed to the effective separation of photo-induced electron–hole by the formed heterophase junction with well-matched band structures, which will be discussed later.

It is also worth noting that, although pure $\text{W}_{18}\text{O}_{49}$ shows activity similar to WO_3 under UV-vis irradiation, $\text{W}_{18}\text{O}_{49}/\text{TiO}_2$ is much more active than that of WO_3/TiO_2 (Fig. 4b and d). The effect of structure should be excluded because both WO_3 and $\text{W}_{18}\text{O}_{49}$ possess similar surface area and morphology. Therefore, the defect chemistry (oxygen vacancies) of $\text{W}_{18}\text{O}_{49}$ may account for the higher photoactivity of $\text{W}_{18}\text{O}_{49}/\text{TiO}_2$ hybrid.

3.3. Photoactivity under visible light

To further elucidate the synergy between $\text{W}_{18}\text{O}_{49}$ and TiO_2 , the photodegradation of MO and phenol were conducted under visible light, respectively (Fig. 5). In this case, only $\text{W}_{18}\text{O}_{49}$ can be excited to generate electron–hole pairs and shows photoactivity, whereas the activity of TiO_2 is negligible. As expected, adding small amount of TiO_2 (W_W from 100 to 90 wt%) can promote the activity of $\text{W}_{18}\text{O}_{49}$. $\text{W}_{18}\text{O}_{49}$ (90 wt%)/ TiO_2 shows the highest activity, which is 1.19 (1.38) times of pure $\text{W}_{18}\text{O}_{49}$ and 1.31 (1.52) times of the benchmark for the degradation of MO (phenol). Furthermore, the hybrids with different composition are always more active than the benchmark, which suggests that the synergy between $\text{W}_{18}\text{O}_{49}$ and TiO_2 also exists under visible light, and the charge transfer from $\text{W}_{18}\text{O}_{49}$ to TiO_2 must happen.

Similar to the photodegradation under UV-vis light, both individual $\text{W}_{18}\text{O}_{49}$ and $\text{W}_{18}\text{O}_{49}/\text{TiO}_2$ hybrid show much higher activity than the counterpart involving WO_3 . Besides the role of oxygen defective surface, the extended visible light absorption may also contribute to the improved activity.

3.4. Photocatalytic active species

The active species typically involved in the photodegradation include holes (h^+), hydroxyl radicals ($\cdot\text{OH}$) and superoxide radicals ($\cdot\text{O}_2^-$). To determine the major active species responsible for the photodegradation of $\text{W}_{18}\text{O}_{49}/\text{TiO}_2$ hybrid, a series of controlled experiments were performed using different radical scavengers, as shown in Fig. 6. Firstly, when TBA (a scavenger for $\cdot\text{OH}$) is added, the degradation of MO keeps almost unchanged, indicating there is no direct relationship between the degradation and $\cdot\text{OH}$ radicals. It

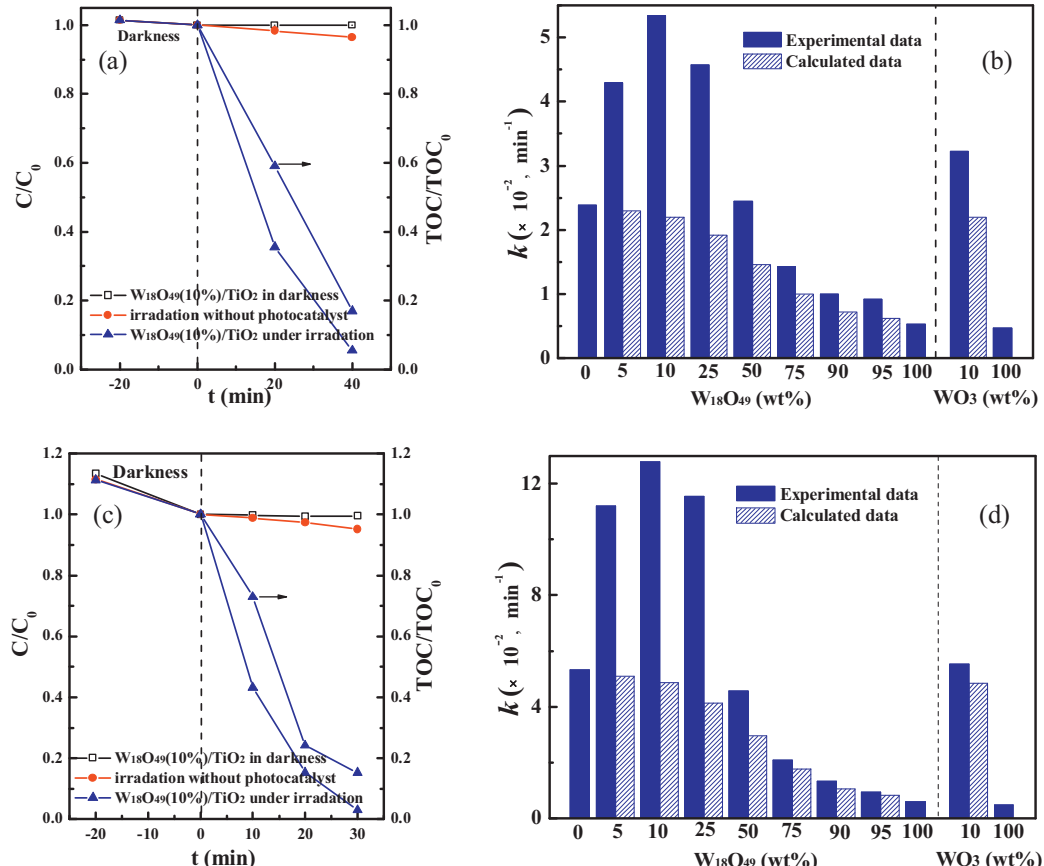


Fig. 4. Photoactivity (experimental data) and the calculated activity of $\text{W}_{18}\text{O}_{49}/\text{TiO}_2$ and WO_3/TiO_2 in degradation of (a and b) MO and (c and d) phenol under UV-vis light.

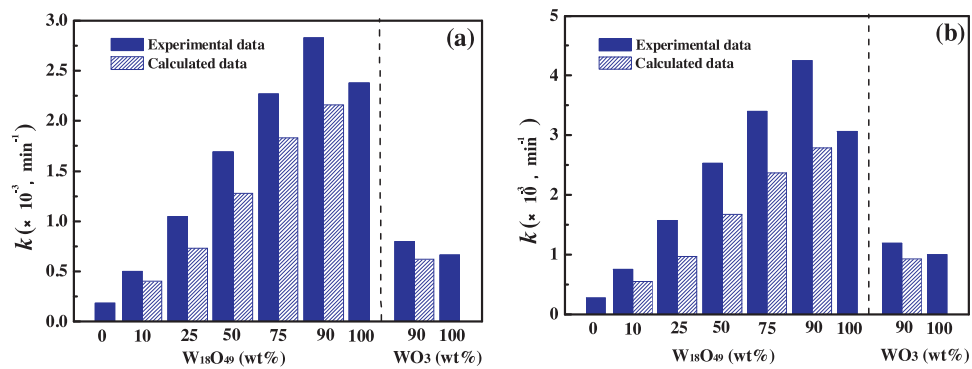
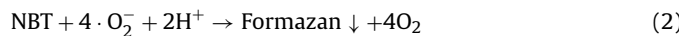


Fig. 5. Photoactivity (experimental data) and the calculated activity of W₁₈O₄₉/TiO₂ and WO₃/TiO₂ in degradation of (a) MO and (b) phenol under visible light.

is a little surprising because lots of literatures report that ·OH are the major active species determining the photodegradation activity [1–3,5]. However, the results of recent literatures that studying the degradation of MO over TiO₂ are in agreement with our findings [24,34]. This suggests that the photocatalytic reaction is subjected to the specific photocatalyst and reaction environment (i.e., the redox potential of holes and the type of reactants) applied. Alternatively, when AO (a scavenger for h⁺) is added, the degradation of MO is decreased moderately, indicating that the h⁺ plays an important role in the degradation via direct oxidizing MO adsorbed on the surface instead of indirect oxidizing via ·OH in aqueous solution. Notably, when BQ, a scavenger for ·O₂[−], is added, the degradation of MO is almost inhibited, illustrating the ·O₂[−] formed via the reduction of O₂ by photo-induced electrons are the key active species in the present photocatalytic reaction.

Considering the importance of ·O₂[−] in the present work, NBT reacting solely with ·O₂[−] was used as a probe to quantify the ·O₂[−] generated from photocatalytic reaction. The formation rate was calculated according to the following reaction: (Eq. (2))



As shown in Fig. 7, the formation rate of ·O₂[−] changes with the composition of W₁₈O₄₉/TiO₂ in a way identical to the photodegradation of MO (see Fig. 5). This gives direct evidence that the ·O₂[−] plays a determinative role in the photodegradation of MO.

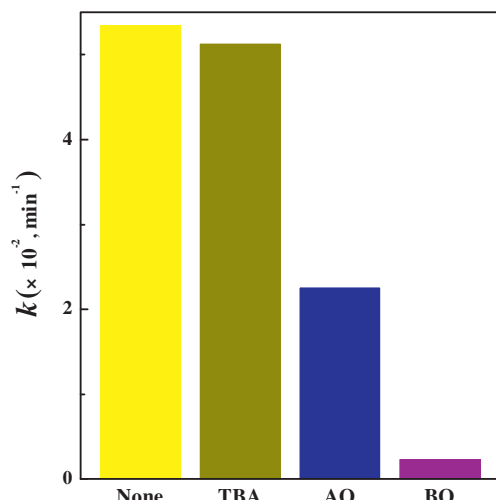


Fig. 6. Effect of scavengers on the photoactivity of W₁₈O₄₉(10 wt%)/TiO₂ under UV-vis light.

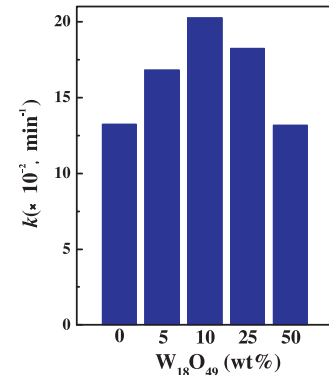
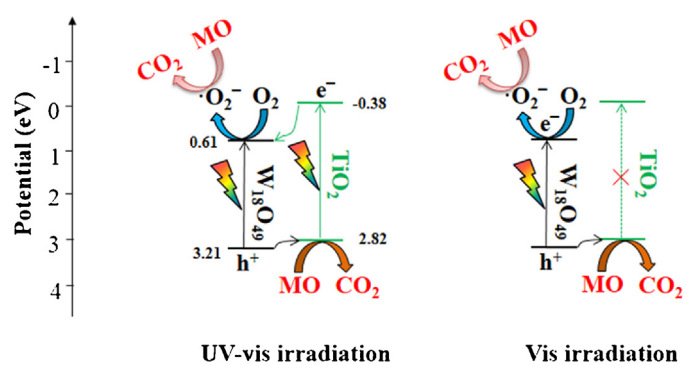


Fig. 7. Formation rate of ·O₂[−] generated over W₁₈O₄₉/TiO₂ under UV-vis light.

3.5. Charge transfer and separation mechanism

As mentioned above, the synergy between W₁₈O₄₉ and TiO₂ in the hybrid should be attributed to the enhanced photo-induced charge separation. According to previous reports [21,22,34], the CB and VB potentials of W₁₈O₄₉ are +0.61 and +3.21 eV (vs. NHE), whereas those of TiO₂ are −0.38 and +2.82 eV (vs. NHE), respectively. Therefore, the band structures of W₁₈O₄₉ and TiO₂ can match very well, providing a charge-transfer pathway between them, with electrons moving to W₁₈O₄₉ and holes to TiO₂ (Scheme 1), respectively. The high surface area of urchin-like W₁₈O₄₉ can increase the possibility of contacting with TiO₂, so simple mixing can produce enough charge transfer interface.

Besides the enhanced photo-induced charge transfer and separation, the defect chemistry (oxygen defects) of W₁₈O₄₉ is a critical issue account for the high activity of the hybrids. It is already reported that, the strong reductive capability of oxygen defects



Scheme 1. Schematic diagram of photo-induced charge transfer and separation over W₁₈O₄₉/TiO₂ hybrid.

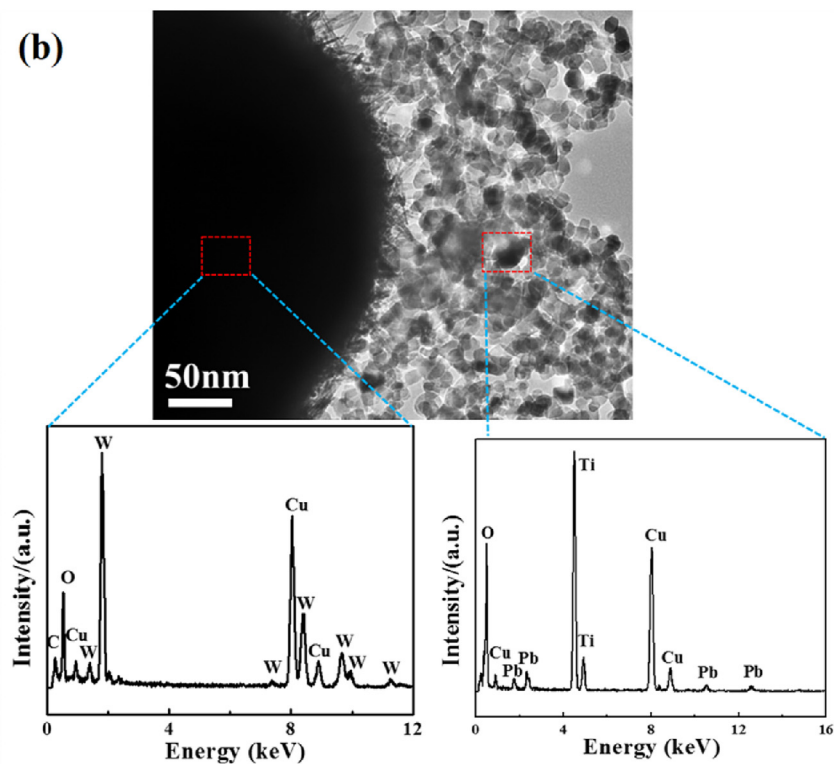
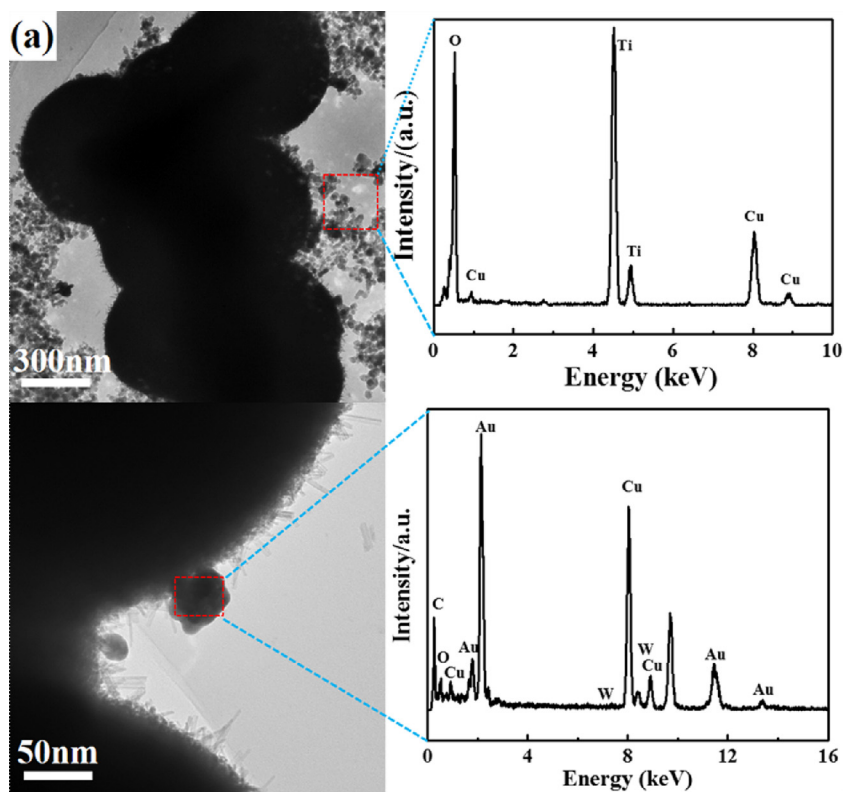


Fig. 8. TEM images and EDX spectra of (a) Au- and (b) PbO₂-deposited W₁₈O₄₉(10 wt%)/TiO₂.

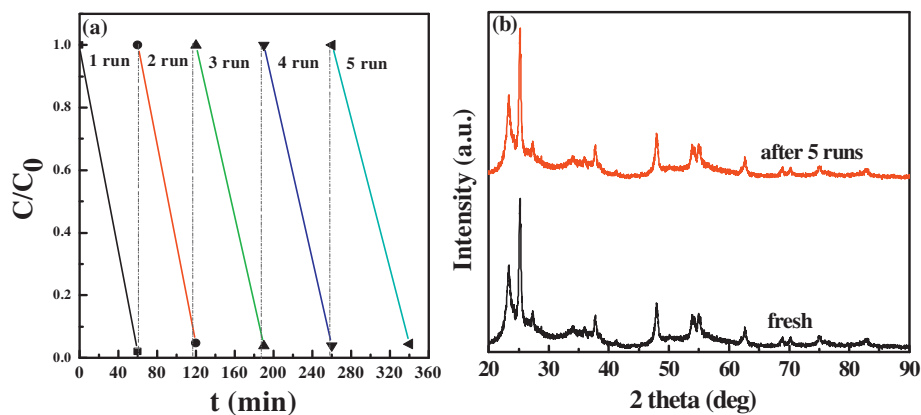


Fig. 9. (a) Cycling of MO degradation over $W_{18}O_{49}$ (10 wt%)/ TiO_2 under UV-vis light and (b) XRD patterns before and after the cycling.

endow $W_{18}O_{49}$ higher activity for CO_2 reduction when compared with WO_3 [19]. The redox potentials (E^0) for eight-electron reduction of CO_2 to CH_4 that is the lowest potentials required for CO_2 reduction is -0.24 eV NHE at $pH = 7$ [1,2]. It is noted that the E^0 for one-electron reduction of O_2 to $\cdot O_2^-$ is -0.28 eV vs. NHE at $pH = 7$, very close to that of CO_2 reduction [25,34]. Naturally, O_2 can be easily reduced to $\cdot O_2^-$ in the present photodegradation. In addition, the high surface area of $W_{18}O_{49}$ can provide more sites trapping O_2 and reducing them into $\cdot O_2^-$. This explains why $\cdot O_2^-$ becomes the key active species and why $W_{18}O_{49}/TiO_2$ is much more active than WO_3/TiO_2 .

The spatial charge separation within the hybrids is further confirmed by photodeposition of Au and PbO_2 , as shown in Fig. 8. The big and dark particles are $W_{18}O_{49}$ and the small particles are TiO_2 . Small Au particles are observed on $W_{18}O_{49}$ surface, and no Au is observed on TiO_2 according to EDX analysis. Although no PbO_2 particles are seen on TiO_2 (probably because of the small particles size), EDX analysis does detect Pb existing in the TiO_2 area but no presence of Pb on $W_{18}O_{49}$. Cu present in all EDX analysis is the substrate of grid supporting the photocatalyst. This result clearly supports that the photo-induced electrons and holes are accumulated on $W_{18}O_{49}$ and TiO_2 for photo-reduction and photo-oxidation, respectively.

3.6. Photostability

The oxygen-defective $W_{18}O_{49}$ is not stable and prone to be oxidized by photo-induced holes, with color changed from blue to yellow [19]. In $W_{18}O_{49}/TiO_2$, this problem can be avoided because the holes in $W_{18}O_{49}$ are transferred to TiO_2 . To evaluate the photostability of $W_{18}O_{49}/TiO_2$, the cycling of photodegradation of MO under UV-vis light was conducted, as shown in Fig. 9. After five cycles, the photoactivity exhibits no obvious loss. As shown in the XRD patterns, both the intensities and positions of the diffractive peaks after the cycling are identical to the fresh counterpart. Also, the hybrid keeps original blue color. This result confirms that $W_{18}O_{49}$ is very stable in the present hybrids.

4. Conclusions

$W_{18}O_{49}/TiO_2$ hybrids show significant synergistic promotion on the photoactivity, due to the well-matched band energies of the two individuals that improves the photo-induced charge transfer and separation with electrons moving to $W_{18}O_{49}$ and holes to TiO_2 . The spatial charge separation also inhibits the self-oxidation of $W_{18}O_{49}$ and gives excellent photostability. $W_{18}O_{49}/TiO_2$ is much more active than WO_3/TiO_2 attributed to the inherent good reductive

capability and wide visible light absorption of oxygen vacancies in $W_{18}O_{49}$. In addition, $\cdot O_2^-$ and hole, especially the former, are the active species inducing the photodegradation of MO.

Acknowledgments

The authors appreciate the supports from the National Natural Science Foundation of China (21222607), the Foundation for the Author of National Excellent Doctoral Dissertation of China (200955) and the Program for New Century Excellent Talents in Universities (NCET-09-0594).

References

- [1] M.A. Henderson, Surf. Sci. Rep. 66 (2011) 185–297.
- [2] A. Kubacka, M. Fernandez-Garcia, G. Colon, Chem. Rev. 112 (2012) 1555–1614.
- [3] G. Liu, L.-C. Yin, J. Wang, P. Niu, C. Zhen, Y. Xie, H.-M. Cheng, Energy Environ. Sci. 5 (2012) 9603–9610.
- [4] X.H. Zhang, U. Veikko, J. Mao, P. Cai, T.Y. Peng, Chem. Eur. J. 18 (2012) 12103–12111.
- [5] R. Rahal, A. Wankhade, D. Cha, A. Fihri, S. Ould-Chikh, U. Patil, V. Polshettiwar, RSC Adv. 2 (2012) 7048–7052.
- [6] L. Pan, J.-J. Zou, X. Zhang, L. Wang, Ind. Eng. Chem. Res. 49 (2010) 8526–8531.
- [7] J.-J. Zou, Y. Liu, L. Pan, L. Wang, X. Zhang, Appl. Catal. B-Environ. 95 (2010) 439–445.
- [8] L. Pan, J.-J. Zou, X. Zhang, L. Wang, J. Am. Chem. Soc. 133 (2011) 10000–10002.
- [9] C. Chen, W. Zhao, P. Lei, J. Zhao, N. Serpone, Chem. Eur. J. 10 (2004) 1956–1965.
- [10] L. Pan, J.-J. Zou, S. Wang, Z.-F. Huang, X. Zhang, L. Wang, Appl. Surf. Sci. 268 (2013) 252–258.
- [11] H.R. Jafry, M.V. Liga, Q. Li, A.R. Barron, Environ. Sci. Technol. 45 (2010) 1563–1568.
- [12] I.-C. Kang, Q. Zhang, S. Yin, T. Sato, F. Saito, Environ. Sci. Technol. 42 (2008) 3622–3626.
- [13] Q. Xiang, J. Yu, M. Jaroniec, Chem. Soc. Rev. 41 (2012) 782–796.
- [14] L. Qi, J. Yu, M. Jaroniec, Phys. Chem. Chem. Phys. 13 (2011) 8915–8923.
- [15] Z. Liu, Z. Hu, H. Huang, Q. Zhang, T. Zhang, J. Zhai, L. Jiang, J. Mater. Chem. 22 (2012) 22120–22125.
- [16] Y. Huo, X. Yang, J. Zhu, H. Li, Appl. Catal. B-Environ. 106 (2011) 69–75.
- [17] X. Yu, S. Liu, J. Yu, Appl. Catal. B-Environ. 104 (2011) 12–20.
- [18] K.E. deKrafft, C. Wang, W. Lin, Adv. Mater. 24 (2012) 2014–2018.
- [19] G. Xi, S. Ouyang, P. Li, J. Ye, Q. Ma, N. Su, H. Bai, C. Wang, Angew. Chem. Int. Ed. 51 (2012) 2395–2399.
- [20] G. Xi, J. Ye, Q. Ma, N. Su, H. Bai, C. Wang, J. Am. Chem. Soc. 134 (2012) 6508–6511.
- [21] S. Sun, X. Chang, L. Dong, Y. Zhang, Z. Li, Y. Qiu, J. Solid State Chem. 184 (2011) 2190–2195.
- [22] F. Kojin, M. Mori, Y. Noda, M. Inagaki, Appl. Catal. B-Environ. 78 (2008) 202–209.
- [23] F. Kojin, M. Mori, Y. Noda, M. Inagaki, Chem. Lett. 35 (2006) 388–389.
- [24] Y. Zhang, N. Zhang, Z.-R. Tang, Y.-J. Xu, Chem. Sci. 4 (2013) 1820–1824.
- [25] Y. Wang, K. Deng, L. Zhang, J. Phys. Chem. C 115 (2011) 14300–14308.
- [26] R. Li, F. Zhang, D. Wang, J. Yang, M. Li, J. Zhu, X. Zhou, H. Han, C. Li, Nat. Commun. 4 (2013) 1432–1439.
- [27] Z. Bian, T. Tachikawa, W. Kim, W. Choi, T. Majima, J. Phys. Chem. C 116 (2012) 25444–25453.

- [28] Z. Zheng, B. Huang, J. Lu, X. Qin, X. Zhang, Y. Dai, *Chem. Eur. J.* 17 (2011) 15032–15038.
- [29] T. Taguchi, Y. Saito, K. Sarukawa, T. Ohno, M. Matsumura, *New J. Chem.* 27 (2003) 1304–1306.
- [30] C.S. Guo, S. Yin, M. Yan, M. Kobayashi, M. Kakihana, T. Sato, *Inorg. Chem.* 51 (2012) 4763–4771.
- [31] C.S. Guo, S. Yin, Q. Dong, T. Sato, *RSC Adv.* 2 (2012) 5041–5043.
- [32] G. Xi, B. Yue, J. Cao, J. Ye, *Chem. Eur. J.* 17 (2011) 5145–5154.
- [33] T. Nütz, M. Haase, *J. Phys. Chem. B* 104 (2000) 8430–8437.
- [34] W. Li, D. Li, Y. Lin, P. Wang, W. Chen, X. Fu, Y. Shao, *J. Phys. Chem. C* 116 (2012) 3552–3560.